# Assessment of approximations in nonequilibrium Green's function theory

T. Kubis*
*Network for Computational Nanotechnology, Birk Nanotechnology Center, School of Electrical and Computer Engineering, Purdue University, West Lafayette, Indiana 47907, USA*

P. Vogl
*Walter Schottky Institute, Technische Universität München, Am Coulombwall 3, D-85748 Garching, Germany*
(Received 3 February 2011; published 5 May 2011)

A nonequilibrium Green's function (NEGF) method for stationary carrier dynamics in open semiconductor nanodevices is presented that includes all relevant incoherent scattering mechanisms. A consistent lead model is developed that ensures all observables to reflect intrinsic device properties. By restricting the charge self-consistent calculations to vertical transport through heterostructures, the Green's functions and self-energies can be determined very accurately. This allows us to assess many commonly used approximations, such as ballistic leads, decoupling of Dyson's and Keldysh's equations, truncated or momentum-averaged self-energies, and local self-energies in the NEGF formalism in detail, and to study limiting cases such as diffusive transport in resistors. The comparison of exact and approximated NEGF calculations illustrates the physical implications and validity of common approximations and suggests numerically efficient simplifications.

DOI: 10.1103/PhysRevB.83.195304 PACS number(s): 72.10.−d, 72.20.Dp, 72.20.Ht

## I. INTRODUCTION

The realistic prediction of carrier dynamics in state-of-the-art semiconductor devices requires a scheme that treats carrier interferences, coherent tunneling, and quantum confinement as well as energy and momentum relaxation on an equal footing. In addition to approaches based on the Pauli master equation and the density matrix formalism,[1–4] the nonequilibrium Green's function (NEGF) method is among the most widely employed methods to describe carrier dynamics in open quantum systems.[5,6] In fact, the NEGF method has been applied successfully to a great variety of systems ranging from phonon transport,[7,8] spin transport,[9,10] electron[11,12] dynamics in metals,[13–16] organic molecules and fullerenes,[17–20] and semiconductor nanostructures.[21–23] Unfortunately, the basic NEGF equations are complex, mathematically cumbersome, and their numerical solution is extremely demanding. Therefore, a wide range of different approximations for particular devices and situations have been developed and employed that make it difficult to judge their adequacy for other problems. In addition, suitable boundary conditions for current-carrying nanometer devices that account for a finite current density in the leads have not been studied in detail in terms of this method yet. As a consequence, the validity of the NEGF method in some limiting cases such as simple resistors is still debatable.

In this paper, a fully self-consistent implementation of the NEGF method for open nanodevices is presented and used to assess the most common approximations employed in this method's implementation. These approximations have been discussed up to now only for very specific device applications. In this paper, we attempt to provide concrete and general guidelines for advisable simplifications.

The most common approximation in NEGF calculations is to set to zero all scattering processes altogether. This is equivalent of solving the Schrödinger or Lippmann-Schwinger equation with open boundary conditions and describes ballistic transport. This approximation can be adequate for low temperatures and high mobilities.[24–27] Another very common and numerically efficient scheme is the Büttiker-probe model, where one replaces the individual physical scattering mechanisms by a global energy and momentum absorbing self-energy.[28–32] Once incoherent scattering is taken into account, it has to be included in the total simulation domain, i.e., in the device and its surroundings, to avoid artificial interferences at the device boundaries. This has been shown for local scattering mechanisms, and we verify this finding also for nonlocal scattering events.[29,33] For quantum cascade structures that consist of hundreds of quantum wells in an external electric field, it is common to use periodic boundary conditions rather than treating the system as a scattering problem with attached asymptotic leads.[34–36] This procedure simplifies the NEGF calculations significantly as well, but is adequate only for field-periodic device structures with sufficient energy dissipation. Another common approximation is to solve only those parts of the NEGF equations that determine the resonance and bound-state energies and sidestep the calculation of the occupation numbers, i.e., the Keldysh equations.[37] In some cases, this approximation has been found to violate Pauli's principle,[37] but more detailed investigations of this interesting ansatz have not been performed so far. Another numerically time-saving approximation that has been used for superlattice calculations replaces the momentum dependence of the phonon- and other scattering potentials by suitable averages.[34,38,39] Finally, important insight into the NEGF method has been obtained by comparing the results of NEGF calculations for Wannier-Stark-type ladder systems and quantum cascade structures with semiclassical Monte Carlo calculations.[38,40,41] Whether these results also apply to typical resistive devices $n$-$i$-$n$ or quantum-well structures will be one of the focuses of the present paper.

While we analyze most of the above-mentioned approximations in equilibrium, another very common approximation affects nonequilibrium situations with a finite current density

 

in the device: It is very common to assume the leads of open devices to remain in equilibrium irrespective of a finite device current. Nevertheless, it is well known that such an approximation generates electrostatic charges at the device-lead interfaces.[27,42–44] Therefore, several models have been developed to compensate these charges. In high resistive devices, it is common to compensate transferred charges by adjusting the chemical potentials of the Fermi distributions within the leads. At higher device current densities, however, it has been suggested to avoid equilibrium electron distributions within the leads to account for current conservation beyond the device boundaries.[42,44–46] Most of the later approaches implement a shifted Fermi distribution for the lead electrons. Typically this shift is calculated within a drift-diffusion model with a given lead electron mobility.[42,44,45,47,48] The nature of transport in nanoscale devices is strongly dependent on the device details and can vary from diffusive to ballistic. Therefore, we extend in this paper the lead model of shifted lead Fermi distributions so that a detailed knowledge of the carrier mobility is no longer required. Instead, the shift of the lead electron distribution is determined such that surface charges at the device-lead boundaries are exactly compensated. Thus, our lead model ensures that the calculated physical observables, and particularly the $I$-$V$ characteristics, reflect intrinsic properties of the device. It is finally shown that the NEGF method yields correct results in the limiting case of diffusive transport by a comparison with solutions of the Boltzmann equation.

In Sec. II A, we briefly introduce the governing equations. In Sec. II B, a lead model is introduced that specifies the boundary conditions for the electrostatic potential and the Green's functions, respectively. The entire Sec. III is devoted to a careful examination and assessment of common approximations of the NEGF method. The consequences of using ballistic leads are presented in Sec. III A. The crucial property of current conservation is lost when self-energies are truncated, as shown in Sec. III B. While in some cases the decoupling of the Dyson and Keldysh equations leads to unphysical results, we discuss situations in Secs. III C and III D in which this approximation can be justified. The consequences of neglecting the nonlocal nature of the Green's functions is discussed in Sec. III E and their momentum dependence is analyzed in Sec. III F. In Sec. III G, three different lead models are discussed and compared to one another. The capability of the NEGF method to reproduce results of semiclassical calculations is demonstrated in Sec. III H. Finally, we summarize our findings in Sec. IV.

## II. METHOD

### A. Fundamentals

To set up our notation and be able to assess various approximations, we briefly summarize the NEGF in this section. We focus on stationary vertical transport in laterally homogeneous quantum-well heterostructures and consider such a device to be in contact with two charge reservoirs at $z = R$ and $z = L$, respectively. Thereby, we consider charge transport as a scattering problem from source to drain with the open device forming the scattering center. The electronic structure is represented in terms of a single-band effective-mass model with an effective mass that may depend on the growth coordinate $z$ as well as on the energy $E$ in order to be able to incorporate nonparabolicity effects. The single-band conduction-electron Hamiltonian is given by

$$H_0 = \frac{-\hbar^2}{2}\frac{\mathrm{d}}{\mathrm{d}z}\frac{1}{m^*(z,E)}\frac{\mathrm{d}}{\mathrm{d}z} + \frac{\hbar^2 k_\parallel^2}{2m^*(z,E)} + V(z),$$
$$V(z) = E_c(z) - e\Phi(z), \tag{1}$$

where $k_\parallel$ is the lateral electron momentum, $\Phi(z)$ the electrostatic potential, and $E_c(z)$ denotes the material- and position-dependent conduction-band edge, including the band offsets. Within the NEGF formalism, stationary transport in open quantum-mechanical systems is characterized by four coupled partial differential equations for the electronic retarded and lesser Green's functions $G^R, G^<$, respectively.[49] In operator form, they read

$$G^R = (E - H_0 - \Sigma^R)^{-1},$$
$$G^< = G^R \Sigma^< G^{R\dagger},$$
$$\Sigma^< = G^< D^<,$$
$$\Sigma^R = G^R D^R + G^R D^< + G^< D^R. \tag{2}$$

Here, $D$ is the sum of all environmental Green's functions that incorporate phonons, impurities, and interface roughness, and $\Sigma$ denotes the self-energies. The solutions of Eqs. (2) in real space do not require one to solve an eigenvalue problem. Therefore, an energy-dependent mass in the Hamiltonian $H_0$ does not increase the complexity of the solution. All Green's functions $G(z,z',k_\parallel,)$ and self-energies $\Sigma(z,z',k_\parallel,E)$ are taken as functions of two spatial coordinates $z,z'$, the lateral momentum $k_\parallel$, and the energy $E$. Once the Green's functions are known, the observables such as the spatially resolved density $n(z)$ and the current density $j(z)$ can be determined straightforwardly,

$$n(z) = \int \mathrm{d}E\, n(z,E)$$
$$= \frac{2}{(2\pi)^3}\mathrm{Im}\int \mathrm{d}E \int \mathrm{d}\vec{k}_\parallel G^<(z,z,k_\parallel,E), \tag{3}$$

$$j(z) = -\frac{\hbar e}{(2\pi)^3}\lim_{z'\to z}\int \mathrm{d}E \int \mathrm{d}\vec{k}_\parallel \frac{1}{m^*(z,E)}$$
$$\times \mathrm{Re}\left(\frac{\mathrm{d}}{\mathrm{d}z} - \frac{\mathrm{d}}{\mathrm{d}z'}\right) G^<(z,z',k_\parallel,E). \tag{4}$$

If not explicitly stated otherwise, we take into account inelastic acoustic and polar-optical-phonon scattering, scattering by charged impurities, rough interfaces, and the electron-electron interaction in the Hartree approximation. The scattering self-energies are determined in the self-consistent Born approximation including their full nonlocal momentum and energy dependence.[50] Taking into account scattering to infinite order is a prerequisite for obeying current conservation exactly.[50] In the real-space basis employed in this work, we exemplify the general, nonlocal retarded, and lesser scattering self-energies for polar-optical-phonon (pop) and charged impurity (imp)

scattering, respectively,[37]

$$\Sigma^{<}_{\rm pop}(z,z',k_\parallel,E) = \frac{\gamma\pi}{(2\pi)^3}\int {\rm d}\vec{l}_\parallel\, V_{\rm pop}(z,z',|\vec{k}_\parallel-\vec{l}_\parallel|)[n_0 G^{<}(z,z',l_\parallel,E-\hbar\omega_0)+(1+n_0)G^{<}(z,z',l_\parallel,E+\hbar\omega_0)], \tag{5}$$

$$\Sigma^{R}_{\rm pop}(z,z',k_\parallel,E) = \frac{\gamma\pi}{(2\pi)^3}\int {\rm d}\vec{l}_\parallel\, V_{\rm pop}(z,z',|\vec{k}_\parallel-\vec{l}_\parallel|)\Bigg[(1+n_0)G^{R}(z,z',l_\parallel,E-\hbar\omega_0)+n_0 G^{R}(z,z',l_\parallel,E+\hbar\omega_0)$$
$$+\frac{1}{2}G^{<}(z,z',l_\parallel,E-\hbar\omega_0)-\frac{1}{2}G^{<}(z,z',l_\parallel,E+\hbar\omega_0)+i\mathcal{P}\int\frac{{\rm d}E'}{2\pi}\left(\frac{G^{<}(z,z',l_\parallel,E')}{E-E'-\hbar\omega_0}-\frac{G^{<}(z,z',l_\parallel,E')}{E-E'+\hbar\omega_0}\right)\Bigg],$$

$$V_{\rm pop}(z,z',k_\parallel) = \frac{{\rm e}^{-\sqrt{k_\parallel^2+q_D^2}|z-z'|}}{\sqrt{k_\parallel^2+q_D^2}}\left(1-\frac{q_D^2|z-z'|}{2\sqrt{k_\parallel^2+q_D^2}}-\frac{q_D^2}{2\left(k_\parallel^2+q_D^2\right)}\right), \tag{6}$$

$$\Sigma_{\rm imp}(z,z',k_\parallel,E) = \frac{e^4}{16\pi^2\varepsilon_0^2\varepsilon_r^2}\int {\rm d}\vec{q}_\parallel\, V_{\rm imp}(z,z',|\vec{k}_\parallel-\vec{q}_\parallel|)G(z,z',q_\parallel,E), V_{\rm imp}(z,z',k_\parallel) = \int {\rm d}z''\, N_D(z'')\frac{{\rm e}^{-\sqrt{q_D^2+k_\parallel^2}(|z-z''|+|z'-z''|)}}{q_D^2+k_\parallel^2}. \tag{7}$$

In these equations, $q_D$ denotes the inverse Debye screening length, $N_D(z)$ is the ionized impurity concentration, and $n_0$ denotes the equilibrium Bose phonon number at the chosen temperature. We note that the contribution of the principal value integral in Eq. (6) is small in laterally homogeneous heterostructures and can be neglected.[34,35] The expression for $\Sigma_{\rm imp}$ holds for both the retarded and the lesser self-energy and contains the same type of Green's function, i.e., $\Sigma^R_{\rm imp}\propto G^R, \Sigma^<_{\rm imp}\propto G^<$. The polar-optical Fröhlich coupling constant $\gamma$ is given by

$$\gamma = e^2\frac{\hbar\omega_0}{2\varepsilon_0}\left(\frac{1}{\varepsilon_\infty}-\frac{1}{\varepsilon_r}\right), \tag{8}$$

where $\omega_0$ is the constant optical-phonon frequency, and $\varepsilon_r$, $\varepsilon_\infty$ are (device averaged values of) the static and dynamic dielectric constant, respectively.[51] These two scattering self-energies reflect all important properties of self-energies that we will discuss in the subsequent sections.

### B. Lead model for open devices

Since we focus on open quantum systems, we need to augment the system of Eqs. (2) for the Green's functions by suitable boundary conditions, i.e., by a consistent treatment of the leads. Given the fact that full NEGF calculations can only be performed for very small nanoscale semiconductor structures at this time, different treatments of the leads are major sources of discrepancy between different models. We will therefore present our lead model in some detail and discuss the effect of different models on observable device properties in the next section.

We consider open, laterally homogeneous devices with electrons in a single parabolic conduction band and attach a semi-infinite lead to the left and to the right of the structure, respectively. Our main goal in setting up a lead model is to make sure the physics is controlled by the interior of the device rather than the leads. Physically, this is only possible if the charge density near the device-lead interface is sufficiently high to screen the electric fields within the device so that it is reasonable to assume flat band boundary conditions. Given this premise, we assume furthermore that the lead-device interfaces are sufficiently smooth not to cause significant reflections or interference effects. We note that the present lead model can be generalized to fully three-dimensional devices with any number of leads, as we show in the Appendix.

In our model, each semi-infinite lead $\ell\in\{L,R\}$ is characterized by a constant effective mass $m^*_\ell$, position-independent electron density $n_\ell$ corresponding to a chemical potential $\mu_\ell$, and a constant electrostatic potential $\Phi_\ell$. The bottom of the conduction band in each lead is denoted by $E_{c,\ell}$. To get reflectionless contacts, i.e., smooth device-lead transitions, we extend the device density of states adjacent to the leads continuously into the leads.

For this purpose, the device Green's functions are calculated including the contact self-energies $\Sigma^R_{\rm con}$ and $\Sigma^<_{\rm con}$. This requires that we include scattering within the leads to the extent that we solve the retarded surface Green's function of the lead self-consistently with $\Sigma^R$ of the device, but assume a fixed electron distribution.[52] This scheme is analogous to the one proposed in Ref. 53, but we maintain the full off-diagonal character of the self-energies across the lead-device interface and replace the scalar elements of the contact self-energy algorithm in Ref. 53 by matrices. The size of these matrices is given by the finite range of the scattering self-energies in the device. The resulting set of nonlinear equations is then solved iteratively.[53]

Within the device, we solve the Poisson equation

$$\varepsilon_0\frac{\rm d}{{\rm d}z}\varepsilon_r(z)\frac{{\rm d}\Phi(z)}{{\rm d}z} = e[n(z)-N_D(z)] \tag{9}$$

self-consistently with all Green's functions in the device. Note that global charge neutrality of the device requires $\varepsilon_{r,L}\Phi'_L = \varepsilon_{r,R}\Phi'_R$ or simply $\Phi'_L=\Phi'_R$ for a single material device, as follows from integration of Eq. (9). Since we assume a high carrier density near the contacts, we use the stronger conditions

$$\text{(I)}\quad \left.\frac{{\rm d}\Phi(z)}{{\rm d}z}\right|_{z=R} = 0, \tag{10}$$

$$\text{(II)} \quad \left.\frac{\mathrm{d}\Phi(z)}{\mathrm{d}z}\right|_{z=L} = 0.$$

In *equilibrium*, i.e., for zero applied bias, we assume the electronic distribution within the leads to be given by equilibrium Fermi distributions. Depending on the device details, our electrostatic boundary conditions (I) and (II) may result in a finite built-in potential across the device,

$$V_{\text{built-in}} = e[\Phi_L - \Phi_R]_{\text{equilibrium}}. \tag{11}$$

We assume the potential $V_{\text{built-in}}$ to remain the same in nonequilibrium situations.

In a *nonequilibrium* situation, charge is transferred from the source to the drain side of the device. Without any compensation, this charge transport results in a dipole at the device boundaries: a positive charge at the source and a negative charge at the drain sided boundary of the device. It is well known that such a dipole prohibits the applied bias to drop completely within the device.[1,27,42,44,45] To compensate this charge dipole at the device boundaries, we assume shifted Fermi distributions within the leads.[1,42,44,45] Accordingly, the electron distribution in lead $\ell$ reads

$$f_\ell(k_\parallel, k_{D,\ell}, E, \mu_\ell) = \{\exp[\beta(\tilde{E}_\ell - \mu_\ell)] + 1\}^{-1}, \tag{12}$$

with

$$\tilde{E}_\ell = \frac{\hbar^2}{2m^*_\ell}[k_\parallel^2 + (k_{z,\ell}(E) - k_{D,\ell})^2]. \tag{13}$$

Hereby, the sign of the variable $k_{D,\ell}$ depends on the direction of the electron flux through the contact. It shifts the center of the lead's Fermi sphere parallel to the average electron momentum in the growth direction,

$$k_{z,\ell}(E) = \sqrt{2m^*_\ell(E - E_{c\ell} - e\Phi_\ell)/\hbar^2 - k_\parallel^2}. \tag{14}$$

With the current flowing from source to drain, $k_{D,\ell}$ is positive in the source and negative in the drain. The shift of the Fermi spheres within the leads causes charge dipoles at both lead boundaries: the source sided lead faces a positive charge at the boundary to the (metallic) reservoir and a negative charge at the boundary with the device; The dipole of the drain sided lead has an opposite configuration. In this way, the shift of the lead Fermi spheres allows us to move the dipole charges to the lead-reservoir interfaces and to guarantee a given bias drop within the device. Therefore, we iteratively determine the two shifts $k_{D,\ell}$ of the Fermi distributions in the two leads with the NEGF results within the device until the two conditions hold,

$$\text{(III)} \quad V_{\text{applied}} = e[\Phi_L - \Phi_R] - V_{\text{built-in}} = \mu_L - \mu_R,$$
$$\text{(IV)} \quad \left|\frac{k_{D,L}}{k_{D,R}}\right| = \frac{m^*_L n_R}{m^*_R n_L}. \tag{15}$$

Please note that these two conditions unambiguously define the two unknown variables $k_{D,L}$ and $k_{D,R}$. Condition (III) guarantees that only one global dipole persists, i.e., the dipole between source and drain reservoir. Then, the total applied bias $V_{\text{applied}}$ completely drops within the device. Condition (IV), on the other hand, mimics current conservation from the leads into the device by assuming that the current density within lead $\ell$ is proportional to $k_{D,\ell}n_\ell/m^*_\ell$.[44] Expression (IV) avoids the introduction of a mobility and is plausible for both diffusive and ballistic situations. In weakly doped and low resistive devices, the shift $k_{D,\ell}$ may grow to values larger than $k_{z,\ell}$ for all energies $E$ of occupied states that would lead to artificial results. This limit is approximately reached when $k_{D,\ell}$ equals the Fermi vector. We therefore restrict its values to the range $|k_{D,\ell}| \leqslant \sqrt[3]{3\pi^2 n_\ell}$. An assessment of this lead model is given in Sec. III G.

## III. RESULTS AND ASSESSMENT OF COMMON APPROXIMATIONS

In this section, we are going to assess several common approximations for the self-consistent solution of the NEGF equations (2). It turns out that the Green's function approach is quite sensitive to some simplifications but less sensitive to others, and in most cases these findings are counterintuitive. We hope that this discussion illustrates the strengths and weaknesses of the NEGF apparatus and eventually contributes to reduced numerical effort and more robust and reliable predictions based on this method.

### A. Ballistic leads

An obvious approximation in any NEGF calculation of open devices is to attach ballistic leads to the structure and include scattering only within the active device. This greatly simplifies the calculations since the surface Green's functions of ballistic leads are analytically known.[54–58] Figure 1 shows the results of two different NEGF calculations of a piece of homogeneously $n$-doped GaAs of 50 nm length with attached GaAs "leads" on both sides and in the absence of any applied bias. Physically, this device simply represents homogeneous bulk GaAs in equilibrium that we have artificially divided into a "device" and two semi-infinite "leads." The doping concentration is $n = 10^{17}$ cm$^{-3}$ and the lattice temperature is set to 300 K. Correct calculations must obviously yield a constant electron density throughout the device. Indeed, Fig. 1 shows a constant electron density (solid line) but only in the case in which scattering has been included within the leads

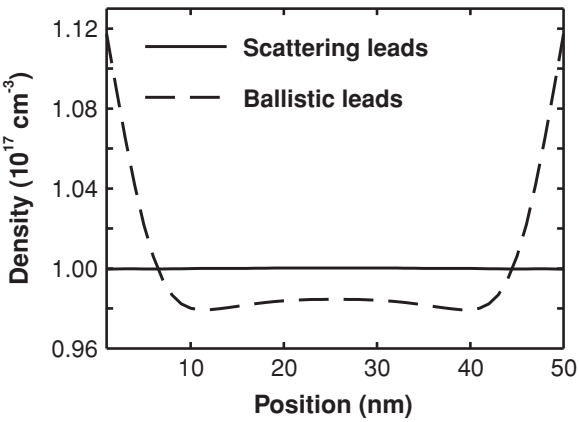


FIG. 1. NEGF calculations of equilibrium electron density in a homogeneously $n$-doped GaAs device with $n = 10^{17}$ cm$^{-3}$ at 300 K. The dashed line shows results for leads with ballistic electrons. They generate interference effects and nonhomogeneous densities. A consistent NEGF implementation (solid line) must include scattering within the leads.

self-consistently. By contrast, if we attach ballistic GaAs leads to the piece of GaAs, the mismatch in the electronic density of states within the leads and within the device causes significant interferences to occur near the device-lead interfaces, which results in an inhomogeneous electron density (dashed line). This result is a consequence of the density of states to be controlled by the retarded Green's function, which contains the scattering self-energies. Therefore, a smooth, reflectionless interface requires matching the density of states between the device and the leads. This, in turn, requires a self-consistent calculation of surface Green's functions. Similar findings have been reported for slightly simplified NEGF calculations with scattering self-energies limited to local on-site scattering.[29,33]

### B. Low-order self-energies

In the absence of vertex corrections to the self-energy that we have not included in the present implementation, we will first show that current conservation can only be guaranteed by implementing only self-energies that contain only fully scattered Green's functions. The most common scheme to achieve this self-consistency is the self-consistent Born approximation. We will show this requirement by considering the following very simple momentum- and energy-conserving model self-energy:

$$\Sigma^{\Lambda} = \alpha \mathbf{G}^{\Lambda}, \tag{16}$$

where $\alpha$ represents a scalar coupling constant that represents some type of perturbation and the index $\Lambda$ labels the three types of Green's functions and self-energies, $\Lambda \in \{<, R, A\}$. The matrix notation for $G$ and $\Sigma$ applies to the spatial coordinates $(z,z')$, whereas the momentum and energy coordinates $\vec{k}_{\parallel}, E$ remain unchanged for this kind of coupling self-energy. The spatial derivative of the current density is given by[54]

$$\frac{\mathrm{d}}{\mathrm{d}z} j(z)\bigg|_{z_0} = -\frac{e}{h(2\pi)^2} \int \mathrm{d}E \int \mathrm{d}^2 k_{\parallel} I(z_0, z_0, k_{\parallel}, E), \tag{17}$$

where the integrand $\mathbf{I}$ reads in matrix form

$$\mathbf{I} = \Sigma^{<}\mathbf{G}^{A} - \mathbf{G}^{<}\Sigma^{A} + \Sigma^{R}\mathbf{G}^{<} - \mathbf{G}^{R}\Sigma^{<}. \tag{18}$$

When we truncate the perturbation series at the order $n$, the integrand $\mathbf{I}$ reads

$$\mathbf{I}_n = \alpha\left[\mathbf{G}^{<}_{n-1}\mathbf{G}^{A}_{n} - \mathbf{G}^{<}_{n}\mathbf{G}^{A}_{n-1} + \mathbf{G}^{R}_{n-1}\mathbf{G}^{<}_{n} - \mathbf{G}^{R}_{n}\mathbf{G}^{<}_{n-1}\right]. \tag{19}$$

The Green's function of consecutive scattering orders only agrees in the limit $n \to \infty$, i.e., in the self-consistent Born approximation

$$\lim_{n\to\infty} \mathbf{G}^{\Lambda}_{n} = \lim_{n\to\infty} \mathbf{G}^{\Lambda}_{n-1}. \tag{20}$$

Only in this limit does the integrand in Eq. (19) vanish and the current is exactly conserved. In any finite order $n$, on the other hand, the integrand is nonzero and can lead to substantial variations of the current density along the device direction $z$.[37] We note that additional approximations may be applied for the Green's functions in some situations that can restore the current conservation in a truncated series expansion of the Green's functions.[37,59] A violation of current conservation has led some researchers to call the integral of Eq. (18) a scattering current $j_{\mathrm{scatt}}$ and define a "total" current to be the sum of $-j_{\mathrm{scatt}}(z)$ and the correct current density $j(z)$ of Eq. (4).[60] While this quantity is spatially constant indeed, it bears no relation to the matrix element of the quantum-mechanical velocity operator and does not represent a converged result for the observable current density.[61] We therefore believe that the NEGF formalism provides no simple way to avoid an infinite summation over self-energies, i.e., the calculation of full Green's functions, particularly in situations where the current density is a crucial quantity.[62] Finally, there is a subtlety to consider very close to the lead-device interface. While we have applied the self-consistent Born approximation in all calculations, the assumption of an analytic electron distribution within the leads causes a violation of current conservation very close to the lead-device interfaces since the self-energies are nonlocal. As a consequence, the current density cannot be exactly conserved in the range of this nonlocality around the device-lead interface. Fortunately, we find this violation of the current conservation to be very small and we typically achieve a relative current conservation of better than $10^{-4}$.

### C. Decoupled retarded and lesser Green's functions

One of the cumbersome as well as numerically most demanding features of the NEGF formalism is the coupled system of Dyson and Keldysh equations. In particular, any retarded self-energy $\Sigma^{R}$ associated with an inelastic-scattering mechanism involves the lesser Green's function $G^{<}$. This raises the question of whether we can obtain a reasonable approximation by leaving out all parts in $\Sigma^{R}$ that contain $G^{<}$. In this way, the system Eqs. (2) would get reduced to two independent sets of equations, which grossly reduces the effort of solving them. Such an approximation effectively implies an independent determination of the resonant state energies and their occupancies. If all state occupancies are small, such an approximation appears to be reasonable, but Lake *et al.* have pointed out that this approximation may violate Pauli blocking.[37] In this section, we will quantitatively analyze the effect of this decoupling of the Dyson and Keldysh equations in a concrete example.

We have performed an exact as well as a decoupled NEGF calculation of the retarded and lesser functions in a laterally homogeneous, nanometer-sized heterostructure with attached GaAs-type leads. The total length of the device is 50 nm, with a 16 nm intrinsic region embedded in between two 17nm $n$-doped regions with $n = 10^{18}$ cm$^{-3}$ each. Within the intrinsic region, there is a 12 nm $In_{0.14}Ga_{0.86}As$ quantum well of 150 meV depth. To illustrate the occupation of bound states, we define a function $f(z,k_{\parallel},E)$,

$$f(z,k_{\parallel},E) \equiv -iG^{<}(z,z,k_{\parallel},E)/A(z,z,k_{\parallel},E), \tag{21}$$

with the spectral function

$$A(z,z',k_{\parallel},E) = i[G^{R}(z,z',k_{\parallel},E) - G^{R\dagger}(z,z',k_{\parallel},E)]. \tag{22}$$

In equilibrium, the function $f(z,k_{\parallel},E)$ can be shown to be equal to the Fermi distribution $f(E,\mu)$.[49] Note that this function does not reflect the density of states but only the energy- and position-dependent occupation function. It turns out that the imaginary part of $f(z,k_{\parallel},E)$ vanishes and its real part is independent of $k_{\parallel}$. Clearly, one expects the function

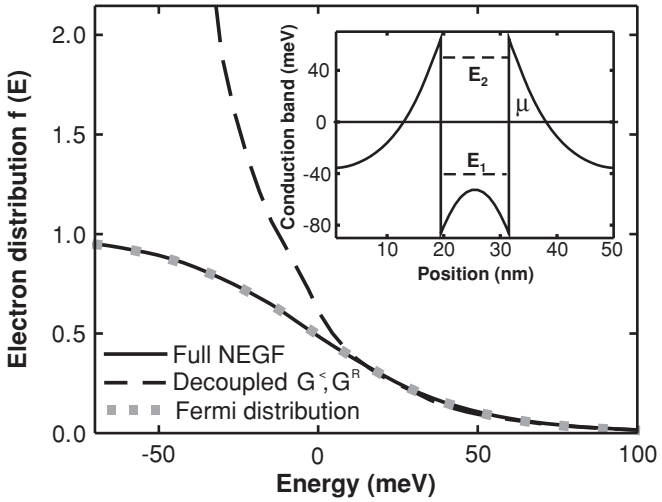


FIG. 2. Equilibrium electron distribution within a 12-nm-wide GaAs/$In_{0.14}Ga_{0.86}As$ quantum well embedded in $n$-doped GaAs at 300 K calculated with fully self-consistent NEGF (solid line) and with decoupled retarded and lesser Green's functions (dashed), respectively. The zero in energy marks the chemical potential $\mu$. The full NEGF result faithfully yields the Fermi distribution (gray dots), in contrast to the decoupled model, which violates the Pauli principle. The inset shows the conduction-band edge along the device with a bound state $E_1$ and a resonance state $E_2$.

$f(z,k_\parallel,E)$ to be independent of position $z$. Indeed, this is the case if the coupling between lesser and retarded functions is fully accounted for, but not so in the decoupled case.

Figure 2 shows the Fermi distribution (gray dots) and the real part of the function $f(z,k_\parallel,E)$ in the exact (solid line) and the approximated (dashed line) calculation in the middle of the $In_{0.14}Ga_{0.86}As$ quantum well. The zero in energy marks the chemical potential of the device. If we include the full coupling of $G^R$ with $G^<$, the calculation perfectly reproduces the Fermi distribution. By contrast, the decoupling of the Dyson and Keldysh equations yields a dramatic deviation from the Fermi distribution as soon as any occupancy exceeds a value of 0.3. The function $f$ even exceeds its physical (Pauli blocking) limit of 1 for low-lying energies that are highly occupied. Since we assume a Fermi distribution in the leads, this triggers an artificial spatial inhomogeneity of $f(z,k_\parallel,E)$ when $\Sigma^R$ is approximated to be independent of $G^<$.

### D. Effect of decoupling on Fermi's Golden Rule

To further illustrate the physical implication of the decoupling approximation of $G^R$ with $G^<$, we will compare the polar-optical-phonon scattering rate in bulk GaAs as obtained from a full and decoupled NEGF calculation with Fermi's Golden Rule. The polar optical phonon (LO-phonon) scattering self-energies are given in Eqs. (5) and (6). We consider homogeneously $n$-doped, unbiased GaAs with $n = 2\times10^{18}$ cm$^{-3}$ and set the zero in energy equal to the chemical potential. At zero and room temperature, this implies the band edge to lie at $-86.42$ and $-79.06$ meV, respectively. Even for this bulk system, we stick to the present coordinate system that is adapted to two-dimensional systems, but we have checked that our calculations are able to reproduce the known analytical formulas for the Green's functions in bulk systems.[63] In homogeneous devices, the Green's functions and self-energies depend only on the difference of the propagation coordinates ($\zeta = z - z'$). This allows us to Fourier transform the imaginary part of the retarded self-energy with respect to $\zeta$ and obtain the scattering rate $\Gamma$ (see e.g., Ref. 64),

$$\Gamma(k_\parallel,k_z,E) = -\frac{2}{\hbar}\mathrm{Im}\int \mathrm{d}\zeta\, \exp(ik_z\zeta)\Sigma^R(\zeta,k_\parallel,E). \quad (23)$$

In particular, we will analyze the on-shell scattering rate $\Gamma$ that is obtained by evaluating $\Gamma$ at the vertical electron momentum,

$$k_z = \sqrt{2m^*E/\hbar^2 - E_c - e\Phi - k_\parallel^2}. \quad (24)$$

This yields the on-shell scattering rate of electrons with kinetic energy $\hbar^2(k_\parallel^2 + k_z^2)/2m^*$.

First, we consider temperature $T = 0$ so that only the emission of LO phonons is possible. Electrons at energies higher than the LO-phonon energy $E > \hbar\omega_0$ as well as holes within the conduction band at energies lower than $E < -\hbar\omega_0$ are able to emit polar-optical phonons [see Fig. 3(a)]. By contrast, electrons and holes for intermediate energies $-\hbar\omega_0 < E < \hbar\omega_0$ cannot emit phonons, because their respective final states are fully occupied.[65] Consequently, scattering with LO phonons for electronic states in the interval $[-\hbar\omega_0,\hbar\omega_0]$ is forbidden at $T = 0$. At room temperature, on the other

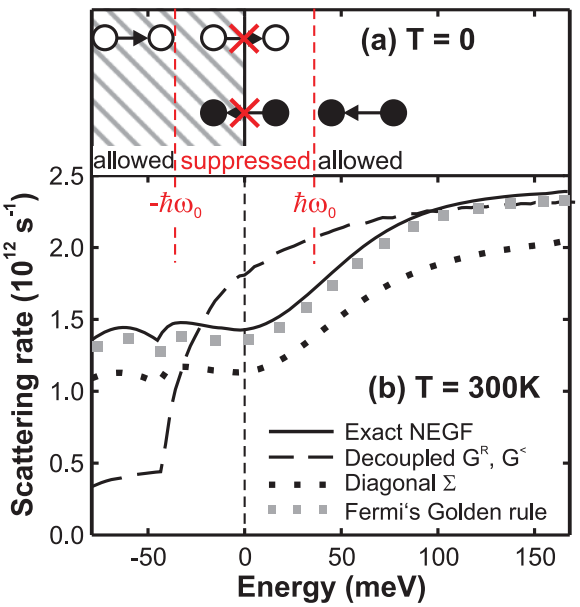


FIG. 3. (Color online) Calculated polar-optical-phonon scattering in homogeneously $n$-doped GaAs with $n = 2\times10^{18}$ cm$^{-3}$ at zero bias. The zero in energy marks the chemical potential. (a) Schematic picture of allowed and forbidden scattering events at $T = 0$. Holes (open circles) and electrons (full circles) can only scatter within the indicated energy windows, set by the optical-phonon energy $\hbar\omega_0$. (b) Total on-shell optical-phonon scattering rate at 300 K. The exact NEGF calculation (solid line) agrees well with Fermi's Golden Rule, i.e., first-order perturbation theory (large gray dots). The dashed line results from NEGF calculations with decoupled retarded and lesser Green's functions. The small black dots depict NEGF calculations where the nonlocality of the self-energy in real space with a spatial resolution of 1 nm has been neglected.

hand, the electron distribution is significantly washed out and LO phonons can both be emitted and absorbed, so that the suppression of scattering within the energy interval of $[-\hbar\omega_0,\hbar\omega_0]$ is less pronounced. The black solid line in Fig. 3(b) shows the polar-optical-phonon scattering rate $\Gamma$ of Eqs. (23) and (6) that results from a fully self-consistent NEGF calculation of this heavily $n$-doped GaAs. For comparison, the gray dots show the scattering rate that results from Fermi's Golden Rule.[51] For the latter, we have explicitly summed over the emission and absorption of LO phonons by electrons as well as the emission and absorption of LO phonons by holes within the conduction band. As one can deduce from this figure, Fermi's Golden Rule closely follows the NEGF result. This implies that higher-order scattering, which is included in the NEGF self-energy, plays only a minor role in equilibrium and bulk GaAs due to the small polar-optical coupling constant. The situation is radically different for the decoupled case. If all terms in the retarded self-energy Eq. (6) that contain $G^<$ are neglected, the scattering of holes in the conduction band as well as the suppression of scattering in the energy interval $[-\hbar\omega_0,\hbar\omega_0]$ are completely absent and the scattering rate is grossly incorrect [see the dashed line in Fig. 3(b)].

In conclusion, we find that the decoupling of inelastic retarded self-energies from $G^<$ is only applicable in situations in which the occupation of all relevant electronic states is smaller than approximately 0.3. Otherwise, many particle effects such as holelike scattering within the conduction band and Pauli blocking become relevant. Even when the state occupancy lies beneath this value, the retarded Green's functions and accordingly the retarded self-energies are influenced by the lesser Green's function via the Poisson potential. This dependence can safely be ignored only in very low-doped devices such as THz quantum cascade lasers.[66]

### E. Local on-site self-energies

In the present real-space basis, all self-energies are nonlocal objects that depend on the two spatial coordinates $z$ and $z'$ independently (see Sec. II A).[37,50,63] This increases the complexity of NEGF calculations significantly[67] and hampers recursive algorithms for the calculation of the Green's functions.[37,53] We therefore investigate here the consequences of limiting self-energies to on-site scattering.[55,56,68] The black dotted line in Fig. 3(b) shows results for the polar-optical-phonon scattering rate of Eq. (23) where only on-site elements $\Sigma(z,z,k_\parallel,E)$, i.e., elements with $\zeta = 0$, have been taken into account. The comparison with the exact NEGF result also shown in this figure shows that nonlocal scattering effects shift the total scattering rate quantitatively, whereas the qualitative trends remain intact, at least in this case. This result is consistent with previous findings for resonant tunneling diodes.[67]

To quantify the nonlocal contributions, Fig. 4 illustrates the imaginary part of the $k_\parallel$-integrated lesser LO-phonon self-energy $\Sigma^<$ in homogeneously $n$-doped bulk GaAs for various energies as a function of the distance $\zeta$ between the two propagation coordinates $z$ and $z'$ (cf. Fig. 3). This self-energy is maximal close to the Fermi energy and decreases for energies above and below it. The dependence of $\Sigma^<$ on the energy $E$ is basically given by the energy-resolved density $n(E)$ [see Eq. (3)] shown in the inset of Fig. 4. Irrespective of the energy, the nonlocal spread of the self-energy in the difference coordinate $\zeta$ extends to approximately three times the device screening length (which amounts to 3 nm for the chosen doping concentration). We find very similar results for the retarded Green's function and for scattering by charged impurities. In devices where the carriers are confined by high barriers such as quantum cascade devices, on the other hand, the nonlocality is essentially limited to the width of the resonant states, i.e., quantum-well widths. This is in agreement with previous findings.[69]

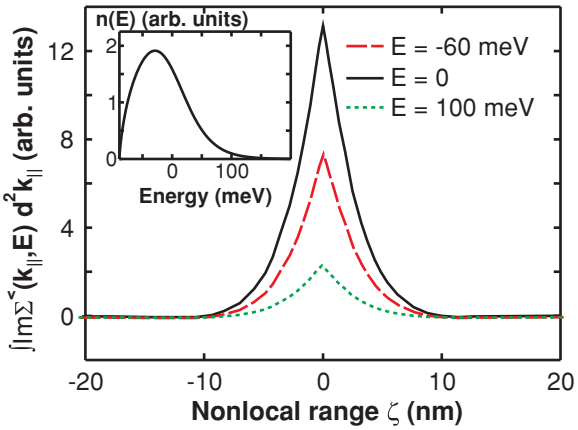


FIG. 4. (Color online) Imaginary part of the lesser self-energy for electronic scattering with polar-optical -phonons in homogeneously $n$-doped GaAs with $n = 2 \times 10^{18}$ cm$^{-3}$ and at room temperature. The self-energy is integrated over the in-plane momentum $k_\parallel$ and shown for various energies relative to the chemical potential as functions of the difference of the two propagation coordinates $\zeta = z - z'$. The spatial resolution is 1 nm, but the lines are drawn continuously. The dependence of $\Sigma^<$ as a function of energy $E$ follows the energy-resolved density that is shown in the inset [see Eq. (3)].

### F. Momentum-averaged self-energies

Since the integrals over the in-plane momentum $l_\parallel$ in Eqs. (5), (6), and (7) are numerically very demanding, it is an obvious and frequently implemented approximation to replace the dependence of the coupling matrix elements $V_{\rm imp}(z,z',k_\parallel)$ and $V_{\rm pop}(z,z',k_\parallel)$ on the momentum transfer $k_\parallel$ by an average value $\Delta q_{\rm typ}$.[34,38] To give an example, the retarded self-energy for the interaction with charged impurities simplifies to

$$\Sigma^R_{\rm imp}(z,z',k_\parallel,E) = V_{\rm imp}(z,z',\Delta q_{\rm typ}) \int {\rm d}l_\parallel l_\parallel G^R(z,z',l_\parallel,E). \tag{25}$$

While this approximation saves a lot of computer time, the energy dependence of different scattering self-energies is no longer specific to the physics of the scattering mechanism.[37] In fact, the remaining energy dependence in the self-energies resembles that for acoustic-phonon scattering and tends to underestimate scattering of low-energy electrons and overestimate it for electrons with high kinetic energies. To further analyze this approximation, we consider the scattering potentials for the LO phonon Eq. (6) and charged impurity scattering Eq. (7) in homogeneous GaAs, respectively. As shown in Fig. 5, the potentials vary significantly with $k_\parallel$.

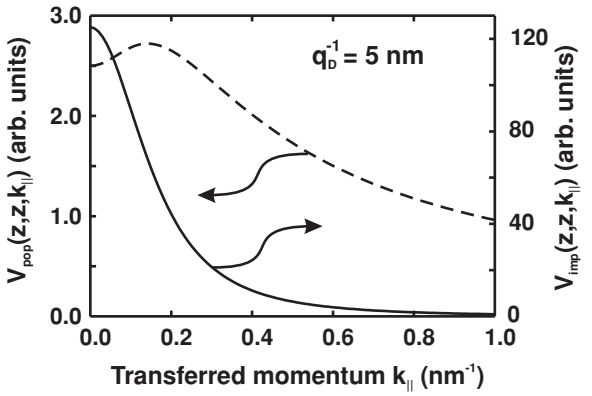


FIG. 5. Calculated scattering potentials for charged impurities (solid) and polar-optical phonons (dashed) at an in-plane momentum $l_{\|} = 0.51$ nm$^{-1}$ as functions of the in-plane momentum $k_{\|}$. The screening length $q_D^{-1}$ is set to 5 nm.

Obviously, the replacement by a constant $\Delta q_{\text{typ}}$ is not advisable and even a redetermination of this value for each voltage for a given device is impractical.[36]

### G. Lead electron distribution

We now discuss the impact of employing different lead models in NEGF calculations for open quantum systems. In particular, let us consider flat band boundary conditions for the potential at the contacts and compare our present lead model that invokes a shifted Fermi distribution (model SF) with a model that employs an unshifted Fermi distribution (model UF).

Concretely, we study an 80-nm-wide laterally homogeneous $n^{++}$-$i$-$n^{+}$ GaAs resistor at a temperature of 50 K. From left to right, we take a 32-nm-wide $n$-doped region with $n = 2 \times 10^{18}$ cm$^{-3}$, followed by a 10.7 nm intrinsic GaAs layer and, finally, a 37.3-nm-wide $n$-doped region with $n = 1 \times 10^{18}$ cm$^{-3}$ [see Fig. 6(a)]. The asymmetry of this structure yields a build-in potential of $V_{\text{built-in}} = -34.2$ meV. By applying a bias voltage of +34.2 mV, both lead conduction-band edges should be exactly equal if the applied voltage drops entirely within the device. For each of the two models, Figs. 6(a) and 6(b) depict the self-consistently calculated electron densities and conduction-band profiles, respectively.

The results for model UF are shown by dotted lines. Figure 6(b) reveals that the difference of the source and drain conduction-band edges in this model is far from zero and does not correctly reflect the applied bias. Indeed, it is known that the assumption of equilibrium electron distributions within the leads causes a charge dipole at the device boundaries and an incomplete bias drop across the device.[42,45]

In contrast, the black solid lines depict results for case SF, which is the presently employed lead model, described in Sec. II B. In this case, the potential drop within the device matches exactly the applied bias voltage. Another important consequence of choosing a shifted Fermi distribution within the leads is shown in Fig. 7. This figure shows the calculated current density for the two lead models UF (dotted line) and SF (solid line), respectively. Since the shifted lead Fermi distributions increase the average electron velocity of the

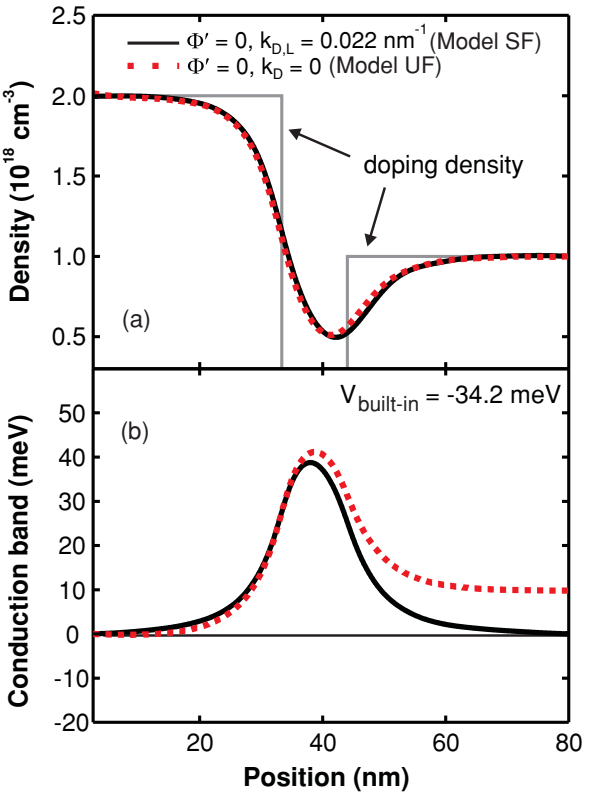


FIG. 6. (Color online) NEGF results for (a) the electron density and (b) the self-consistently determined conduction-band profile for two different lead models. The doping has been chosen so that the built-in potential exactly compensates the applied bias. The conduction-band edges in (b) should therefore lie at zero energy at the device boundaries. The dotted lines correspond to a lead model with equilibrium lead electron distributions and vanishing electric fields at the boundaries (model UF), as described in the main text. The black solid lines show results of the presently proposed lead model SF that includes shifted lead electron distributions.

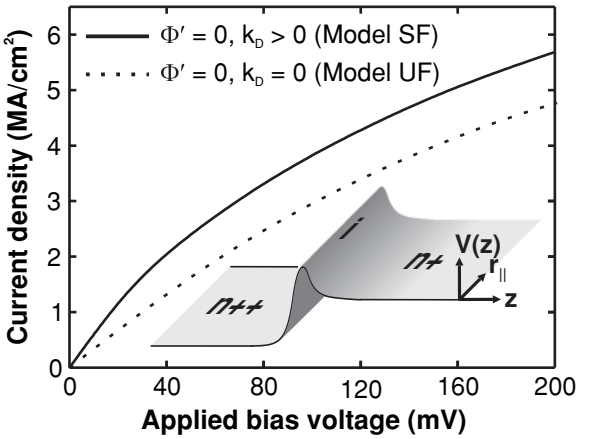


FIG. 7. Current density as a function of applied bias voltage for the same $n^{++}$-$i$-$n^{+}$ resistor as in Fig. 6. NEGF calculations with lead model UF corresponding to equilibrium leads (dotted line) predict significantly smaller current densities than those with the presently proposed lead model SF that is based on self-consistently shifted lead Fermi distributions (solid line).

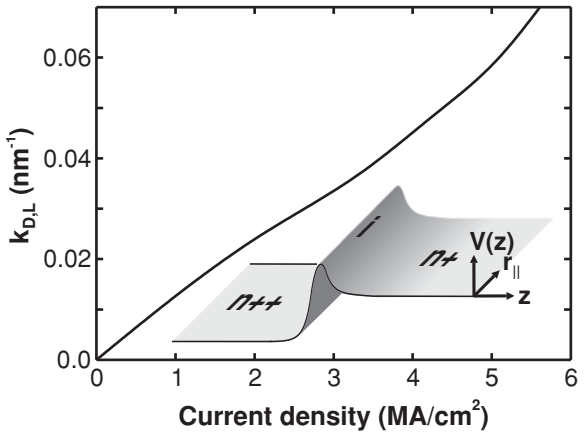


FIG. 8. Self-consistently determined shift of the Fermi distribution in the left contact of the $n^{++}$-$i$-$n^{+}$ resistor of Fig. 6 as a function of current density.

carriers in the device, the current density is larger than in the case of unshifted Fermi distributions.In fact, the low-field mobility $\mu$ is almost twice as large in the currently employed lead model (SF) ($\mu \sim 2286$ cm$^2$ V$^{-1}$ s$^{-1}$) as in model UF with unshifted Fermi distributions ($\mu \sim 1330$ cm$^2$ V$^{-1}$ s$^{-1}$). Part of the reason for this finding lies in the incomplete potential drop within the device.[27,43] In addition, the vanishing average momentum of lead electrons in case UF represents an additional serial resistance that also reduces the current density.

Interestingly, we find the self-consistently determined momentum shifts $k_{D,\ell}$ of the Fermi distribution in the leads to be almost linearly related to the current density. Figure 8 shows $k_{D,L}$ of the present $n^{++}$-$i$-$n^{+}$ structure as a function of the current density. The almost linear relation between the momentum $k_{D,L}$ and current density is consistent with previous lead models and may simplify the determination of a suitable shift of the Fermi distribution.[44]

Finally, we show results that one obtains by not enforcing flat band boundary conditions for the potentials at the contacts and invoking unshifted contact Fermi distributions. For the device we are considering in this section, charge neutrality only dictates the electric field to be the same at both contacts,

$$\left.\frac{\mathrm{d}\Phi(z)}{\mathrm{d}z}\right|_{z=R} = \left.\frac{\mathrm{d}\Phi(z)}{\mathrm{d}z}\right|_{z=L}.$$

We may determine the magnitude of this electric field by requiring the applied potential to drop entirely within the device, i.e., by condition III in Eq. (15). The resulting charge density and conduction-band energy as a function of position within the device is depicted in Fig. 9. This figure reveals an artificial pinch-off near the left device boundary and a charge accumulation near the right boundary, which are clearly artifacts of the chosen lead model. This result is a consequence of the lower average velocity of the carriers within the contacts as compared to the situation within the device, where they get accelerated by the electric field. This clearly demonstrates the importance of a consistent global treatment of the electron distribution both inside the contacts and within the active device region.

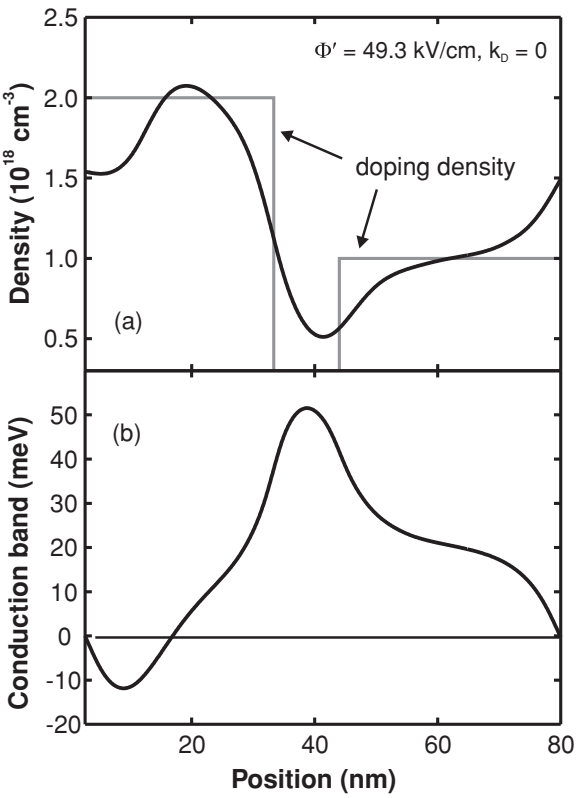


FIG. 9. NEGF results for (a) the electron density and (b) the self-consistently determined conduction-band profile for a lead model with unshifted equilibrium electrons within the contacts but with nonvanishing electric fields at the boundaries. This model leads to unphysical charge depletions and accumulations, as discussed in the main text.

### H. Semiclassical limit

The stationary current characteristics of our simple $n^{++}$-$i$-$n^{+}$ resistor are well described by semiclassical transport, particularly since it is larger than 10 nm in size and does not contain any bound states.[27,31,32] Consequently, a self-consistent NEGF calculation should yield results in close agreement with the solution of the Boltzmann equation, provided we employ the same type of scattering mechanisms and matrix elements. Given the fact that a NEGF calculation is far from being physically transparent, such a comparison is of utmost relevance for judging and understanding the robustness and reliability of the NEGF method. Figure 10 shows the electron density of the present $n^{++}$-$i$-$n^{+}$ resistor that results from the NEGF method (circles) and from the solution of the semiclassical Boltzmann equation (solid line), respectively. The excellent agreement of both results confirms that the NEGF method correctly yields the limiting case of quasiclassical systems. Previous work on stationary electron transport in superlattices and quantum cascade lasers has shown that semiclassical transport models may even agree with NEGF calculations in systems with confined states, when the transport is dominated by incoherent scattering.[38,40,41] In passing, we would like to point out that all results in this paper have been obtained within the NEGF approach. A semiclassical calculation has only been performed for the comparison in Fig. 10.

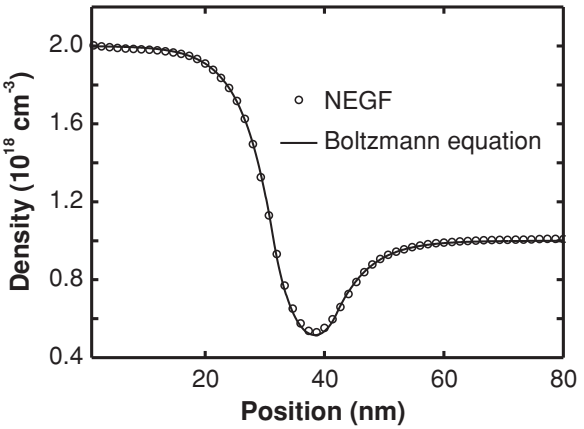


FIG. 10. Equilibrium electron density of the $n^{++}$-$i$-$n^{+}$ GaAs resistor of Fig. 6 for zero bias. The result of the NEGF calculation is depicted by open circles and agrees excellently with the solution of the semiclassical Boltzmann equation (solid line).

## IV. CONCLUSION

In this work, we have implemented and assessed the NEGF method for stationary electron transport in open semiconductor nanodevices by including incoherent scattering on LO and acoustic phonons and charged impurities. All Green's functions are dressed by incorporating scattering to infinite order, and their nonlocal nature as well as their full energy and momentum dependence are taken into account. It has been demonstrated that the electron distribution within the leads must be self-consistently adjusted to the current density in the device in order to obtain physically meaningful results. Our calculations indicate that the density of states within the leads must be matched to that in the device to obtain results that reflect the intrinsic physics of the device. This typically requires the numerical solution of the lead's surface Green's functions. Many frequently implemented approximations have been assessed in some detail. The present study suggests that the coupling between the retarded and lesser Green's function may be neglected when Pauli blocking plays no role, i.e., the state occupancy is less than 30% for all device states. In addition, we have found that the nonlocality of the self-energies in a position basis can be limited to approximately three times the screening length or to the typical extension of confined states in devices with high barriers. Unfortunately, the calculations also showed that the energy and momentum dependence of scattering self-energies is difficult to neglect or approximate. In summary, the present work sheds new light on the strengths and weaknesses of the nonequilibrium Green's functions method that may help in its future applications.

## ACKNOWLEDGMENTS

This work has been supported by the Austrian Scientific Fund FWF (SFB-IRON), the Deutsche Forschungsgemeinschaft (SFB 631 and SPP 1285), the Excellence Cluster Nanosystems Initiative Munich, and the National Science Foundation (Grants No. OCI-0749140, No. EEC-0228390, and No. ECCS-0701612). Computational resources of nanoHUB.org are gratefully acknowledged.

## APPENDIX: GENERALIZED LEAD MODEL

In the following, we generalize the lead model presented in Sec. II B to general device dimensions and an arbitrary number of leads. We separate our system into a device of volume $\Omega$ and its surroundings. We denote the device boundary by $\delta\Omega$ and its surface normal with $\vec{\eta}$. Charge carriers can enter or leave the device through $N$ reservoirs that are coupled to the device via $N$ leads. We use the term contact $\delta\Omega_{c,\ell}$ for the intersection of lead $\ell \in \{1,\ldots,N\}$ and the device and define

$$\delta\Omega_c = \bigcup_{\ell=1}^{N} \delta\Omega_{c,\ell}. \tag{A1}$$

The remaining device surface, i.e.,

$$\overline{\delta\Omega_c} = \delta\Omega \setminus \delta\Omega_c, \tag{A2}$$

acts as a barrier of infinite height. We solve the Poisson equation in the device under the condition of vanishing electric fields *perpendicular* to the device surface,

$$\text{(I)} \quad [\vec{\nabla}\Phi(\vec{x})] \cdot \vec{\eta}(\vec{x})|_{\delta\Omega} = 0. \tag{A3}$$

This condition automatically implies global charge neutrality of the device,

$$\int_{\delta\Omega} \varepsilon(\vec{x})[\vec{\nabla}\Phi(\vec{x})] \cdot \vec{\eta}(\vec{x}) \mathrm{d}\vec{x} = 0. \tag{A4}$$

To guarantee charge neutral leads, the doping density close to $\delta\Omega$ is assumed to be sufficiently high so that all electric fields of the device interior that are parallel to $\vec{\eta}(\vec{x})$ are screened within the device. Please note that the electrostatic fields *parallel to the device surface* may still be finite. In *equilibrium*, we assume the electrons in each lead to be distributed according to a single Fermi function. Still, we allow the self-consistent solution of the electron density and the Poisson equation to result in a finite built-in potential $V_{\text{built-in}}(\vec{x})$ at $\vec{x} \in \delta\Omega$. In *nonequilibrium*, we assign individual chemical potentials $\mu_\ell$ to each lead,

$$\mu_\ell(\vec{x})|_{\delta\Omega_{c,\ell}} = \mu_\ell, \tag{A5}$$

and use the following shifted distribution of electrons in lead $\ell$ (analogous to Sec. II B):

$$f_\ell(\vec{k},E) = \left\{ \exp\left[\beta\left(\frac{\hbar^2}{2m^*_\ell(E)}|\vec{k}-\vec{k}_{D,\ell}|^2 - \mu_\ell\right)\right] + 1 \right\}^{-1}. \tag{A6}$$

Hereby, we assume a homogeneous energy-dependent effective mass $m^*_\ell(E)$ in the lead $\ell$. The vector $\vec{k}_{D,\ell}$ lies perpendicular to the contact,

$$\vec{k}_{D,\ell} = k_{D,\ell}\vec{\eta}_\ell. \tag{A7}$$

The shifts of the lead distributions are determined implicitly from the condition that the bias drops completely within the device,

$$\text{(II)} \quad e\int_{\delta\Omega_{c,\ell}} [\Phi(\vec{x}) + V_{\text{built-in}}(\vec{x})]\mathrm{d}\vec{x} - \mu_\ell = \kappa, (\ell = 1,2,\ldots,N). \tag{A8}$$

To determine the variable $\kappa$, we assume the current density in the lead $\ell$ to be proportional to a product of the shift $k_{D,\ell}$, the inverse energy averaged effective mass $\langle m_\ell^* \rangle^{-1}$, and the electron density $n(\vec{x})$ integrated along the contact area $\delta\Omega_{c,\ell}$. Since the total amount of current density that flows into the device has to flow out of it again, the variable $\kappa$ has to be determined such that the global current is conserved. This leads to the condition

$$\text{(III)} \quad \sum_{\ell=1}^{N} k_{D,\ell} \langle m_\ell^* \rangle^{-1} \int_{\delta\Omega_{c,\ell}} n(\vec{x}) \mathrm{d}\vec{x} = 0. \tag{A9}$$

*tkubis@purdue.edu


[1] M. V. Fischetti, J. Appl. Phys. **83**, 270 (1998).
[2] C. Weber, A. Wacker, and A. Knorr, Phys. Rev. B **79**, 165322 (2009).
[3] H. Willenberg, G. H. Döhler, and J. Faist, Phys. Rev. B **67**, 085315 (2003).
[4] R. C. Iotti and F. Rossi, Phys. Status Solidi B **238**, 462 (2003).
[5] L. P. Kadanoff and G. Baym, *Quantum Statistical Mechanics* (Benjamin, Menlo Park, CA, 1962).
[6] L. V. Keldysh, Sov. Phys. JETP **20**, 1018 (1965).
[7] Y. Xu, J.-S. Wang, W. Duan, B.-L. Gu, and B. Li, Phys. Rev. B **78**, 224303 (2008).
[8] N. Mingo, Phys. Rev. B **74**, 125402 (2006).
[9] M. Yamamoto, T. Ohtsuki, and B. Kramer, Phys. Rev. B **72**, 115321 (2005).
[10] N. Sergueev, Q.-F. Sun, H. Guo, B. G. Wang, and J. Wang, Phys. Rev. B **65**, 165303 (2002).
[11] M. Luisier, A. Schenk, and W. Fichtner, J. Appl. Phys. **100**, 043713 (2006).
[12] V. N. Do, P. Dollfus, and V. L. Nguyen, J. Appl. Phys. **100**, 093705 (2006).
[13] Z. Chen, J. Wang, B. Wang, and D. Y. Xing, Phys. Lett. A **334**, 436 (2005).
[14] Y. Ke, K. Xia, and H. Guo, Phys. Rev. Lett. **100**, 166805 (2008).
[15] W. Belzig, F. K. Wilhelm, C. Bruder, G. Schön, and A. D. Zaikin, Superlatt. Microstruct. **25**, 1251 (1999).
[16] T. Frederiksen, M. Paulsson, M. Brandbyge, and A.-P. Jauho, Phys. Rev. B **75**, 205413 (2007).
[17] T. Sato, K. Shizu, T. Kuga, K. Tanaka, and H. Kaji, Chem. Phys. Lett. **458**, 152 (2008).
[18] P. Damle, A. W. Gosh, and S. Datta, Chem. Phys. **281**, 171 (2002).
[19] H. Li and X. Q. Zhang, Phys. Lett. A **372**, 4294 (2008).
[20] G. Schull, T. Frederiksen, M. Brandbyge, and R. Berndt, Phys. Rev. Lett. **103**, 206803 (2009).
[21] X. Zheng, W. Chen, M. Stroscio, and L. F. Register, Phys. Rev. B **73**, 245304 (2006).
[22] P. Havu, M. J. Puska, R. M. Nieminen, and V. Havu, Phys. Rev. B **70**, 233308 (2004).
[23] M. Lazzeri, S. Piscanec, F. Mauri, A. C. Ferrari, and J. Robertson, Phys. Rev. Lett. **95**, 236802 (2005).
[24] D. Mamaluy, D. Vasileska, M. Sabathil, T. Zibold, and P. Vogl, Phys. Rev. B **71**, 245321 (2005).
[25] T. Zibold, P. Vogl, and A. Bertoni, Phys. Rev. B **76**, 195301 (2007).
[26] B. K. Nikolić, S. Souma, L. P. Zârbo, and J. Sinova, Phys. Rev. Lett. **95**, 046601 (2005).
[27] Z. Ren, R. Venugopal, S. Datta, M. Lundstrom, D. Jovanović, and J. Fossum, IEDM Tech. Digest (2000), pp. 715–718.
[28] M. Büttiker, Phys. Rev. B **33**, 3020 (1986).
[29] S. Sato and N. Sano, J. Comput. Electron. **7**, 301 (2008).
[30] S. Wang and N. Mingo, Phys. Rev. B **79**, 115316 (2009).
[31] M. Lundstrom and Z. Ren, IEEE Trans. Electron Dev. **49**, 133 (2002).
[32] Z. Ren, R. Venugopal, S. Goasguen, S. Datta, and M. Lundstrom, IEEE Trans. Electron Dev. **50**, 1914 (2003).
[33] M. Frey, A. Esposito, and A. Schenk, in *Proceedings of the 13th International Workshop on Computational Electronics (IWCE-13)*, (IEEE, Beijing, 2009), pp. 17–20.
[34] S.-C. Lee and A. Wacker, Phys. Rev. B **66**, 245314 (2002).
[35] N. Vukmirović, Z. Ikonić, D. Indjin, and P. Harrison, Phys. Rev. B **76**, 245313 (2007).
[36] T. Schmielau and M. F. Pereira, Phys. Status Solidi B **246**, 329 (2009).
[37] R. Lake, G. Klimeck, R. C. Bowen, and D. Jovanovic, J. Appl. Phys. **81**, 7845 (1997).
[38] A. Wacker, A.-P. Jauho, S. Rott, A. Markus, P. Binder, and G. H. Döhler, Phys. Rev. Lett. **83**, 836 (1999).
[39] A. Wacker, Phys. Status Solidi C **5**, 215 (2008).
[40] A. Wacker and A.-P. Jauho, Phys. Rev. Lett. **80**, 369 (1998).
[41] A. Mátyás, T. Kubis, P. Lugli, and C. Jirauschek, Physica E **42**, 2628 (2010).
[42] W. Pötz, J. Appl. Phys. **66**, 2458 (1989).
[43] S. Datta, Superlatt. Microstruct. **28**, 253 (2000).
[44] S. E. Laux, A. Kumar, and M. V. Fischetti, J. Appl. Phys. **95**, 5545 (2004).
[45] W. R. Frensley, Rev. Mod. Phys. **62**, 745 (1990).
[46] W. Pötz, J. Appl. Phys. **71**, 2297 (1992).
[47] M. V. Fischetti, Phys. Rev. B **59**, 4901 (1999).
[48] G. Klimeck, J. Comput. Electron. **2**, 177 (2003).
[49] H. Haug and A.-P. Jauho, *Quantum Kinetics in Transport and Optics of Semiconductors* (Springer, Berlin, 1996).
[50] T. Kubis, C. Yeh, P. Vogl, A. Benz, G. Fasching, and C. Deutsch, Phys. Rev. B **79**, 195323 (2009).
[51] B. K. Ridley, *Quantum Processes in Semiconductors* (Oxford Science Publications, Oxford, 1982).
[52] This implies that we approximate the lesser surface Green's function in each lead by $(-1)f(G_S^R - G_S^{R\dagger})$, where $f$ is the lead electron distribution and $G_S^R$ is the retarded surface Green's function.
[53] A. Svizhenko, M. P. Anantram, T. R. Govindan, B. Biegel, and R. Venugopal, J. Appl. Phys. **91**, 2343 (2002).
[54] S. Datta, *Electronic Transport in Mesoscopic Systems* (Cambridge University Press, Cambridge, 1995).
[55] R. Venugopal, M. Paulsson, S. Goasguen, S. Datta, and M. Lundstrom, J. Appl. Phys. **93**, 5613 (2003).
[56] A. A. Yanik, G. Klimeck, and S. Datta, Phys. Rev. B **76**, 045213 (2007).
[57] R. Golizadeh-Mojarad and S. Datta, Phys. Rev. B **75**, 081301(R) (2007).
[58] Y.-S. Liu, H. Chen, X.-H. Fan, and X.-F. Yang, Phys. Rev. B **73**, 115310 (2006).

[59]M. Paulsson, T. Frederiksen, and M. Brandbyge, J. Phys. Conf. Ser. **35**, 247 (2006).
[60]T. Schmielau and M. F. Pereira, Appl. Phys. Lett. **95**, 231111 (2009).
[61]S.-C. Lee, F. Banit, M. Woerner, and A. Wacker, Phys. Rev. B **73**, 245320 (2006).
[62]K. S. Thygesen and A. Rubio, Phys. Rev. B **77**, 115333 (2008).
[63]T. Kubis, *Quantum Transport in Semiconductor Nanostructures*, edited by G. Abstreiter, M. C. Amann, M. Stutzmann, and P. Vogl (Verein zur Förderung des Walter Schottky Instituts der Technischen Universität München e.V., Garching, 2009); [http://nanohub.org/resources/8612].
[64]A. Wacker, Phys. Rep. **357**, 1 (2002).
[65]G. D. Mahan, *Many-Particle Physics* (Plenum, New York, 1990).
[66]A. M. Andrews, A. Benz, C. Deutsch, G. Fasching, K. Unterrainer, P. Klang, W. Schrenk, and G. Strasser, Mater. Sci. Eng. B **147**, 152 (2008).
[67]G. Klimeck, R. Lake, C. L. Fernando, R. C. Bowen, D. Blanks, M. Leng, T. Moise, Y. C. Kao, and W. R. Frensley, in *Proceedings of the International Conference on Quantum Devices and Circuits: Alexandria, Egypt, 1996*, edited by K. Ismail, S. Bandyopadhyay, and J. P. Leburton (World Scientific, London, 1997).
[68]S. Jin, Y. J. Park, and H. S. Min, J. Appl. Phys. **99**, 123719 (2006).
[69]S.-C. Lee, F. Banit, M. Woerner, and A. Wacker, Phys. Rev. B **73**, 245320 (2006).